

## The $a_1(1260)$ as a $\rho\pi$ resonance in nuclear matter

D. CABRERA<sup>1</sup>, D. JIDO<sup>2</sup>, R. RAPP<sup>3</sup> and L. ROCA<sup>4,2</sup>

<sup>1</sup>*Departamento de Física Teórica II, Universidad Complutense, 28040 Madrid, Spain*

<sup>2</sup>*Yukawa Institute for Theoretical Physics, Kyoto University, Kyoto 606-8502, Japan*

<sup>3</sup>*Cyclotron Institute and Physics Department, Texas A&M University, College Station, Texas 77843-3366, U.S.A.*

<sup>4</sup>*Departamento de Física, Universidad de Murcia, E-30071 Murcia, Spain*

We present a theoretical study of the properties of the  $a_1(1260)$  axial-vector resonance in a cold nuclear medium. In the vacuum, the  $a_1(1260)$  resonance is generated dynamically from the interactions of a pseudoscalar and vector meson ( $\rho\pi$  and  $K\bar{K}^*$ ) in a coupled channel chiral unitary approach. Medium effects are implemented through the modification of the  $\rho$  and  $\pi$  propagators at finite nuclear density from well established microscopic many-body calculations. The in-medium pion spectral function accounts for the coupling to  $N$ -hole and  $\Delta$ -hole excitations including short range correlations, whereas the in-medium  $\rho$  incorporates modifications of its virtual pion cloud as well as direct resonance-hole excitations. The resulting in-medium  $a_1(1260)$  exhibits significant broadening with increasing density as reflected in the  $\rho\pi$  scattering amplitude. The possible relation of our results with partial restoration of chiral symmetry in nuclear matter is discussed in terms of in-medium Weinberg sum rules.

### §1. Introduction

The investigation of modifications of hadron properties in nuclear matter has been a vigorous activity in nuclear physics over the past  $\sim 30$  years. The origin of the interest is at least twofold. On the one hand, the modification of the in-medium properties of hadrons has direct impact on the nuclear equation of state, as relevant, for instance, in the description of nuclear saturation,<sup>1)</sup> neutron stars<sup>2)</sup> and low-energy heavy-ion collisions.<sup>3)</sup> On the other hand, it is expected that in-medium hadronic spectral functions encode precursor effects of transitions to new phases of nuclear matter with modified symmetry properties, such as the partial restoration of the chiral symmetry of QCD in nuclear matter.<sup>4),5)</sup> In either case, quantitative evaluations of hadronic spectral properties in a consistent framework are mandatory to realize the pertinent objectives. Large-scale experimental efforts are devoted to search for in-medium modifications especially of mesonic excitations, including pion and dilepton production experiments off nuclear targets,<sup>6)-9)</sup> and dilepton production in heavy-ion collisions.<sup>10)-12)</sup> In particular in the latter, which are mostly sensitive to the in-medium  $\rho$  spectral function, the produced hot and dense QCD medium is expected to evolve to a significant extent in the vicinity of the chiral restoration transition. Thus, to properly interpret the  $\rho$  signal, it is essential to establish its theoretical connection to chiral symmetry.

In the standard interpretation of chiral symmetry, the chiral partner of the vector-isovector current (dominated by the  $\rho$  meson) is identified with the axialvector-

isovector one (dominated by the  $a_1$ , plus a derivative of the pion current)<sup>\*)</sup>. Therefore, if chiral symmetry is restored in the nuclear medium, there should be no difference between left-handed and right-handed currents or, in other words, between vector and axialvector current-current correlators (and spectral functions). This elevates the study of the modification of the axialvector channel to an important theoretical issue, even if its experimental measurement will not turn out to be feasible. Such studies will be helpful in discriminating scenarios of chiral symmetry restoration, which, in principle, can be rather different. E.g., two extreme scenarios for the degeneration of vector and axialvector spectral functions are (i) the vector and axialvector mesons survive as well defined states with a common mass; (ii) both vector and axialvector spectral functions are strongly broadened dissolving any quasiparticle poles (“melting resonance” scenario<sup>14)</sup>).

Thus far relatively few calculations to evaluate the properties of the axialvector resonances in the medium have been performed. In Ref. 15) a schematic “ $a_1$ -sobar” model at finite density has been constructed where an important role is played by the putative chiral partners of the  $\rho$ -sobar resonance-hole excitations (e.g.,  $N(1520)N^{-1}$ , etc.); see also Ref. 16). In Ref. 17), a linear  $\sigma$  model with a global implementation of vector mesons into the chiral pion Lagrangian (as opposed to local ones in the Hidden-Local-Symmetry (HLS) and Massive-Yang-Mills (MYM) approaches) has been constructed and applied at finite temperature. In Ref. 18) finite-temperature studies have been carried out based on different local realizations of chiral symmetry within the HLS scheme. A gauged linear  $\sigma$  model was studied in a selfconsistent mean-field scheme at finite temperature in Ref. 19); see also Ref. 20). In all of these studies the  $a_1$  meson was introduced as a genuine degree of freedom.

In the last few years several works<sup>21)–23)</sup> have reported arguments and evidence for a dynamical nature of low-lying axialvector resonances in vacuum, utilizing variants of the chiral unitary approach.<sup>24)–31)</sup> The latter has been widely and successfully applied to various meson-meson<sup>25)–27), 32)–34)</sup> and meson-baryon<sup>28), 29), 35)–41)</sup> systems, both in vacuum and in cold nuclear matter. One of the main results is that many meson and baryon resonances can be described by meson-meson or meson-baryon dynamics without introducing a genuine field into the hadronic Lagrangian<sup>\*\*)</sup>. Also the axialvector resonances naturally appear<sup>21), 22)</sup> as poles in the scattering matrix of the interaction of pseudoscalar mesons with vector mesons, once coupled channels with the only input of the lowest order chiral Lagrangian are accounted for (including the lowest-lying vector mesons, but without explicit axialvector fields). The low-lying axialvector can be described by dynamics of a pseudoscalar and a vector meson. In particular, the  $a_1(1260)$  can be interpreted as a strongly correlated  $\rho\pi$  system.

In the present work, we combine the picture of a dynamically generated axialvector resonance<sup>22)</sup> with hadronic many-body techniques, to obtain an estimate of the in-medium axialvector spectral function. An advantage of this approach is that

---

<sup>\*)</sup> See, however, Ref. 13) for an alternative interpretation in terms of the so-called vector manifestation.

<sup>\*\*)</sup> Recently a method to test whether dynamically described states can be interpreted as quasi-bound states of hadrons has been proposed in Ref. 42).

one does not have to specify scarcely known couplings of the  $a_1$  to higher resonances (both in scattering off pions at finite temperature and off nucleons at finite density). The medium modifications are implemented in the intermediate unitary loops, specifically via in-medium  $\pi$  and  $\rho$  spectral functions which are rather well known from detailed many-body calculations in connection with comparisons to a wide range of data (both in nuclei and in heavy-ion reactions). Since our model for the (generated)  $a_1(1260)$  is still beset with significant uncertainties even in the vacuum (mainly due to the large  $a_1$  width),<sup>22)</sup> it is not yet warranted to aim at a complete assessment of all possible in-medium effects. Based on previous experience in other meson-meson and meson-baryon systems, we will therefore restrict ourselves to the in-medium renormalization of intermediate pseudoscalar and vector-meson states, which should provide an estimate of the most prominent medium modifications.

Our article is organized as follows: in Sec. 2 we summarize the formalism of pseudoscalar-vector meson interactions in vacuum, which is the starting point for the present calculation, and emphasize its main virtues and uncertainties. The inputs for the pion and  $\rho$ -meson self-energies in cold nuclear matter are discussed in Sec. 3, which we use to describe in some detail how the  $\rho\pi$  2-particle propagator is modified at finite density. Sec. 4 contains our results for the in-medium  $\rho\pi$  scattering amplitude (specifically around the  $a_1(1260)$  pole), as well as an estimate for its impact on partial chiral symmetry restoration by evaluating in-medium Weinberg sum rules. In Sec. 5 we draw conclusions and give an outlook to future lines of investigation.

## §2. The pseudoscalar-vector meson interaction in vacuum

We start by introducing our model for the  $a_1(1260)$  resonance in free space. In Ref. 22) several axialvector resonances are dynamically generated with the only input of the lowest-order chiral Lagrangian and unitarity in coupled channels. Most of the experimentally known low-lying axialvector resonances can be accounted for as emerging from the interaction of a vector ( $V$ ) and a pseudoscalar ( $P$ ) meson, manifesting themselves as poles in unphysical Riemann sheets of the  $VP$  scattering amplitudes.

Considering the vector mesons as fields transforming homogeneously under the nonlinear realization of chiral symmetry,<sup>43)</sup> the interaction of two vector and two pseudoscalar mesons at lowest order in the pseudoscalar fields can be obtained from the following interaction Lagrangian:<sup>44)</sup>

$$\mathcal{L} = -\frac{1}{4}\{(\nabla_\mu V_\nu - \nabla_\nu V_\mu)(\nabla^\mu V^\nu - \nabla^\nu V^\mu)\}, \quad (2.1)$$

where  $\nabla_\mu V_\nu = \partial_\mu V_\nu + [\Gamma_\mu, V_\nu]$  is the  $SU(3)$ -matrix valued covariant derivative, with the  $SU(3)$  connection defined as  $\Gamma_\mu = (u^\dagger \partial_\mu u + u \partial_\mu u^\dagger)/2$ ,  $u = \exp(P/\sqrt{2}f)$  and

$$P \equiv \begin{pmatrix} \frac{\pi^0}{\sqrt{2}} + \frac{\eta_8}{\sqrt{6}} & \pi^+ & K^+ \\ \pi^- & -\frac{\pi^0}{\sqrt{2}} + \frac{\eta_8}{\sqrt{6}} & K^0 \\ K^- & \bar{K}^0 & -\frac{2\eta_8}{\sqrt{6}} \end{pmatrix}, \quad (2.2)$$

$$V_\mu \equiv \begin{pmatrix} \frac{\rho^0}{\sqrt{2}} + \frac{\omega}{\sqrt{2}} & \rho^+ & K^{*+} \\ \rho^- & -\frac{\rho^0}{\sqrt{2}} + \frac{\omega}{\sqrt{2}} & K^{*0} \\ K^{*-} & \bar{K}^0 & \phi \end{pmatrix}_\mu .$$

The Lagrangian of Eq. (2.1) is invariant under chiral transformations  $SU(3)_L \otimes SU(3)_R$ .

For the present work we only need the interaction terms containing two vector and two pseudoscalar mesons. Thus, expanding the Lagrangian of Eq. (2.1) up to two vector and two pseudoscalar fields one obtains<sup>(21), (22)</sup>

$$\mathcal{L}_{VP} = -\frac{1}{4f^2} \langle [V^\mu, \partial^\nu V_\mu] [P, \partial_\mu P] \rangle , \quad (2.3)$$

which allows to evaluate the  $VP \rightarrow VP$  tree level amplitudes. Their explicit expression, after projecting onto  $S$ -waves, reads

$$\epsilon \cdot \epsilon' V_{ij}(s) = -\frac{\epsilon \cdot \epsilon'}{8f^2} C_{ij} \left[ 3s - (M^2 + m^2 + M'^2 + m'^2) - \frac{1}{s} (M^2 - m^2)(M'^2 - m'^2) \right] , \quad (2.4)$$

where  $\epsilon$  ( $\epsilon'$ ) denotes the polarization four-vector of the incoming (outgoing) vector meson. The masses  $M$  ( $M'$ ) and  $m$  ( $m'$ ) correspond to the initial (final) vector mesons and initial (final) pseudoscalar mesons, respectively, and we use an average value for each isospin multiplet. The indices  $i$  and  $j$  represent the initial and final  $VP$  states, respectively, in the isospin basis. The numerical coefficients,  $C_{ij}$ , can be fixed by the  $SU(3)$  flavor symmetry and the values can be found in Ref. 22). For the present study of the  $a_1(1260)$ , we have only two channels; the  $\rho\pi$  channel and the negative  $G$ -parity combination  $1/\sqrt{2}(|\bar{K}^*K\rangle - |K^*\bar{K}\rangle)$ . Note that the tree level amplitude in Eq. (2.4) only depends on the pion decay constant,  $f = 93$  MeV.

The full  $T$ -matrix can now be obtained by unitarizing the tree level amplitudes from the chiral Lagrangian, cf. Eq. (2.4). In Ref. 22) this was carried out within a coupled channel Bethe-Salpeter formalism (equivalent to the Inverse Amplitude Method<sup>(24), (26)</sup>) or the  $N/D$  method<sup>(27)</sup>) for the two-meson interaction. The transverse part of the  $VP \rightarrow VP$  unitarized scattering amplitude, which encodes possibly dynamically generated resonance poles (see Ref. 22) for details), takes the form

$$T = -[1 + VG]^{-1} V \vec{\epsilon} \cdot \epsilon' , \quad (2.5)$$

where the  $V$ -matrix elements are those of Eq. (2.4). The matrix  $G$  is diagonal with the  $l^{\text{th}}$  element,  $G_l$ , given by the two-meson loop function,

$$G_l(P) = i \int \frac{d^4q}{(2\pi)^4} \frac{1}{(P-q)^2 - M_l^2 + i\epsilon} \frac{1}{q^2 - m_l^2 + i\epsilon} , \quad (2.6)$$

where  $P$  is the total four-momentum,  $P^2 = s$ . In the  $\rho\pi$  channel, which is the main channel in building up the  $a_1(1260)$ , the width of the  $\rho$  meson is significant ( $\simeq 150$  MeV). This has been considered in the evaluation of the  $G_{\rho\pi}$  function by replacing the stable-particle vector meson propagator in Eq. (2.6) by the appropriate version accounting for the two-pion decay width (or self-energy). This will be



Fig. 1. Diagrammatic interpretation of the unitarization of the  $VP \rightarrow VP$  amplitude.

discussed in more detail in the next section. Eq. (2.5) represents the resummation of the diagrammatic series shown in Fig. 1.

The energy-momentum integration in Eq. (2.6) for  $G_l$  is divergent and hence has to be regularized. This was done in Ref. 22) in either a cut-off or dimensional regularization scheme. Both methods lead to qualitatively similar results. In the present study we will use a cut-off in the three-momentum of the intermediate particles, which provides a transparent regularization method in a nuclear medium. The regularization procedure introduces the only free parameter of the model,  $q_{\max}$ , which we take of a “natural” size,  $q_{\max} \sim 1$  GeV.

The  $T$ -matrix obtained from Eq. (2.5) contains the information on possible resonances dynamically generated from the  $VP$  interaction. The identification of the resonances and the assignment of their main properties, i.e., mass and width, is not unique. In scattering theory it is common practice to identify resonances with poles on unphysical Riemann sheets of a certain partial-wave amplitude. In Ref. 22), several poles of the  $T$ -matrix in the second Riemann sheet were found which have been associated with the  $a_1(1260)$ ,  $b_1(1235)$ ,  $h_1(1170)$ ,  $h_1(1380)$ ,  $f_1(1285)$  and the two  $K_1(1270)$  resonances. If the pole position is not very far from the real axis and there are no thresholds close by, the real and imaginary parts of the pole position approximately define the mass and half-width of the resonance. For the quantum numbers of the  $a_1(1260)$  channel we find a pole at  $\sqrt{s_{\text{pole}}} = (1117 - i177)$  MeV. This would imply a width of the order of 350 MeV. Note that in the PDG the mass is given as  $M_{a_1} = (1230 \pm 40)$  MeV and the value for the width is quoted with large uncertainty,  $\Gamma_{a_1} \sim 250\text{-}600$  MeV. The unitarized  $VP$  scattering amplitude discussed here has been recently used in a detailed analysis of the  $\tau \rightarrow \pi\pi\pi\nu$  decay spectrum<sup>45),46)</sup> and compared to experimental data from the ALEPH<sup>47)</sup> and CLEO<sup>48)</sup> collaborations. The model reproduces the data well with a single regularization parameter, a momentum cut-off of the same size as used in Ref. 22) and in the present work, and without the need of introducing an explicit  $a_1$  field in the theory. In fact, introducing an explicit  $a_1$  was found to worsen the agreement with experiment unless an “unnatural” choice for the cut-off value is made. The results from Refs. 45), 46) provide a phenomenological test of our dynamically generated  $a_1(1260)$  and increase confidence in the model as a starting point for our calculation in nuclear matter.

As discussed in Ref. 22), we assign to our calculated  $a_1$  pole position an uncertainty of about 100 MeV for the real part and of about 50% for the imaginary part, based on different regularization schemes and the consideration of a finite decay width for the intermediate vector meson. This may not be of too great a concern given that the resonance is far from the real axis and that the experimental width has a large uncertainty. The experimentally accessible information, which is also well defined from a theoretical point of view, is the scattering amplitude on the real

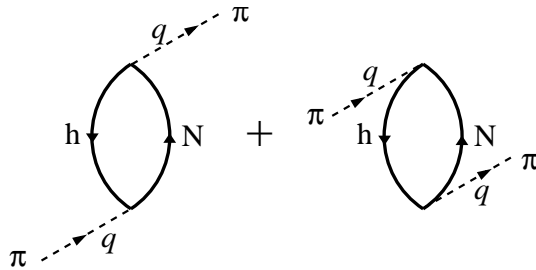


Fig. 2. Particle-hole ( $Nh$ ) excitation diagrams contributing to the  $P$ -wave pion self-energy.

energy axis. Hence, we will base the discussion of our results largely on the  $\rho\pi$  amplitude and its modification due to a finite nuclear density. The estimated values of the mass and decay width of the resonance (extracted from the pole position) are not of much relevance in the present work since we are interested in the relative change in the nuclear medium with respect to the free case. Our aim is to provide an estimation of the modifications that the  $a_1(1260)$  experiences in the nuclear medium as a consequence of many-body dynamics in the intermediate  $\rho\pi$  system.

### §3. Nuclear Medium Modifications

As discussed above, the nuclear medium effects on the dynamically generated  $a_1$  will be restricted to many-body calculations of the  $\rho$  and  $\pi$  self-energies. We neglect medium effects on the hidden strangeness channel as it lies higher in energy and has a weaker coupling to the  $a_1$  spectrum, as we shall see in the next section.

In addition to the modified meson propagators, in-medium vertex corrections to the vacuum  $VP$  interaction, in principle, occur. Vertex corrections play a crucial role, for instance, in restoring transversality of the  $\rho$ -self-energy tensor in nuclear matter.<sup>49)–51)</sup> Another example are scalar-isoscalar  $\pi\pi$  correlations in nuclear matter, where vertex corrections associated with the  $\pi N$  interaction are required by chiral symmetry.<sup>52)</sup> In the present model, we expect vertex corrections to be necessary in connection with the partial conservation of the axial current (PCAC), which should be maintained in the presence of a nuclear medium (especially in scenarios where the system approaches chiral symmetry restoration). The manifestation of PCAC at the level of the  $\rho\pi$  amplitude in our model is not obvious, since correlated  $VP$  exchange only accounts for the (low-energy) resonant part of the axialvector correlator (additional non-resonant (or background) terms, such as uncorrelated  $3\pi$  exchange, have to be included at the same level<sup>46)</sup>). Including vertex corrections in the present model would thus require a systematic analysis of the Lagrangian terms involving pseudoscalar, vector meson and baryon interactions which is beyond the scope of this paper. It shall be addressed in future work within an evaluation of the full axialvector spectral function in nuclear matter. Generally, we expect that in-medium vertex correction enhance the medium effects on the  $\pi\rho$  amplitude and axialvector correlator.

Let us turn to the in-medium pion propagator. In cold nuclear matter, the pion

spectrum exhibits a mixture of the pion quasi-particle mode and predominantly  $P$ -wave nucleon-hole ( $Nh$ ) and Delta-hole ( $\Delta h$ ) excitations,<sup>53),54)</sup> as depicted diagrammatically in Fig. 2 for the  $s$ - and  $u$ -channel  $Nh$  excitation. The lowest-order irreducible  $P$ -wave pion self-energy reads

$$\Pi_\pi^p(q^0, \vec{q}; \varrho) = \frac{\left(\frac{f_N}{m_\pi}\right)^2 F_\pi(\vec{q}^2) \vec{q}^2 [U_{NN^{-1}}(q^0, \vec{q}; \varrho) + U_{\Delta N^{-1}}(q^0, \vec{q}; \varrho)]}{1 - \left(\frac{f_N}{m_\pi}\right)^2 g' [U_{NN^{-1}}(q^0, \vec{q}; \varrho) + U_{\Delta N^{-1}}(q^0, \vec{q}; \varrho)]}, \quad (3.1)$$

where  $U$  denotes the Lindhard function at a nuclear density  $\varrho$ ,<sup>55)</sup> and  $f_N$  ( $f_\Delta$ ) is the  $\pi NN$  ( $\pi N\Delta$ ) coupling constant determined from analyses of pion-nucleon and pion-nucleus reactions,  $f_N \simeq 1$  and  $f_\Delta/f_N \simeq 2.13$  (a factor of  $f_\Delta/f_N$  is absorbed in the definition of the  $\Delta h$  Lindhard function). The strength of the collective modes of the pion is modified by repulsive, spin-isospin  $NN$  and  $N\Delta$  short-range correlations.<sup>53)</sup> In Eq. (3.1) the latter are accounted for in a phenomenological way with a single Landau-Migdal interaction parameter,  $g' = 0.7$ , and the corresponding RPA series for the pion self-energy is resummed (somewhat different couplings for  $NN$ - $N\Delta$  and  $N\Delta$ - $N\Delta$  interactions have been considered, for instance, in Ref. 51)). Eq. (3.1) includes finite-size effects on the  $\pi NN$  and  $\pi N\Delta$  vertices via hadronic monopole form-factors,

$$F_\pi(\vec{q}^2) = \Lambda_\pi^2 / (\Lambda_\pi^2 + \vec{q}^2), \quad (3.2)$$

with  $\Lambda_\pi \sim 1$  GeV.

A more general parameterization of the short-range correlation effects in the pion self-energy is given in Ref. 51), in terms of three different Migdal parameters in a coupled-channel set-up:  $g'_{11}$  ( $NNNN$  vertex),  $g'_{12}$  ( $NNN\Delta$  vertex) and  $g'_{22}$  ( $NN\Delta\Delta$  vertex). One obtains for the pion self-energy

$$\Pi_\pi^p(q^0, \vec{q}; \varrho) = \frac{\left(\frac{f_N}{m_\pi}\right)^2 F_\pi(\vec{q}^2) \vec{q}^2 [U_{NN^{-1}} + U_{\Delta N^{-1}} - (g'_{11} - 2g'_{12} + g'_{22})U_{NN^{-1}}U_{\Delta N^{-1}}]}{1 - \left(\frac{f_N}{m_\pi}\right)^2 [g'_{11}U_{NN^{-1}} + g'_{22}U_{\Delta N^{-1}} - (g'_{11}g'_{22} - g'_{12}{}^2)U_{NN^{-1}}U_{\Delta N^{-1}}]}. \quad (3.3)$$

We shall adopt the parameter values in,<sup>51)</sup> namely,  $g'_{11} = 0.6$ ,  $g'_{12} = g'_{22} = 0.2$  and  $\Lambda_\pi = 0.3$  GeV, which were obtained from an analysis of pion-induced vector-meson production,  $\pi N \rightarrow \rho N$ .<sup>56)</sup> In the following we will denote as  $\pi$ -self-energy B the parameterization in Eq. (3.3) with the parameter values quoted above, and refer to Eq. (3.1) as  $\pi$ -self-energy A with the parameter values quoted thereafter. Using both models A and B for the pion self-energy will give some indication of the uncertainties in our final results for the properties of the  $a_1$  resonance in a nuclear medium.

For the in-medium  $\rho$ -meson self-energy we adopt the approach of Refs. 51), 57) which is based on a realistic description of the  $\rho$  in free space (consistent with  $\pi\pi$   $P$ -wave scattering and the pion electromagnetic form-factor). In cold nuclear matter, the self-energy is built from two components:  $Nh$  and  $\Delta h$  excitations in the two-pion cloud,  $\Pi_{\rho\pi\pi}$ , and direct excitations of baryonic resonances in  $\rho N$  scattering,

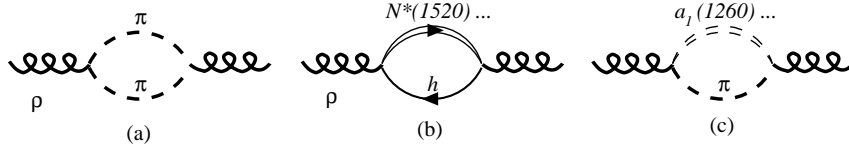


Fig. 3. Contributions to the  $\rho$ -meson self-energy in nuclear matter from the coupling to (a) the two-pion cloud, (b) resonance-hole (“rho-sobar”) excitations, and (c) the pion axialvector system.

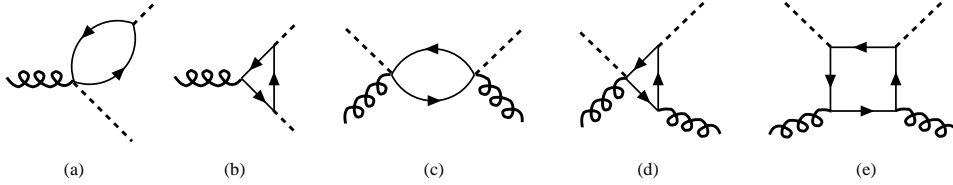


Fig. 4.  $\rho\pi\pi$  vertex corrections, from  $Nh$  and  $\Delta h$  insertions associated to the pion self-energy, accounted for in the two-pion part of the  $\rho$  self-energy.

$\Pi_{\rho Bh}$ , as depicted in Figs. 3 (a) and (b). Since the 4-pion cloud, Fig. 3 (c), is not accounted for in the vacuum  $\rho$  (due its much higher energy threshold), we do not include its nuclear modifications here<sup>\*)</sup>. These contributions have been evaluated in an effective quantum hadro-dynamical model of meson-meson and meson-baryon interactions, both in cold<sup>51)</sup> and hot<sup>14), 58)</sup> hadronic matter. For the first component,  $\Pi_{\rho\pi\pi}$ , special care needs to be taken to preserve the Ward-Takahashi identities of the vector meson propagator, which requires a complete set of vertex correction diagrams, as illustrated in Fig. 4. Note that the pion-cloud modifications have been computed at finite 3-momentum which is essential for the applications in the present paper. For the second component of the  $\rho$  self-energy,  $\Pi_{\rho Bh}$ , a set of  $\sim 10$  baryonic resonances has been accounted for; of particular relevance is the  $N^*(1520)$ , which strongly couples to  $S$ -wave  $\rho N$  states. The parameters underlying the total  $\rho$  self-energy have been quantitatively constrained by a fit of photoabsorption cross sections on the proton and nuclei,<sup>57)</sup> as well as of total  $\pi N \rightarrow \rho N$  cross sections.

At this point it is in order to comment on the difference in the values used for  $\Lambda_\pi$  between models A and B of the pion self-energy. The hard form-factor with  $\Lambda_\pi \sim 1$  GeV represents a typical value used in meson-exchange potentials of the  $NN$  force where the pion figures as a space-like degree of freedom (smaller values of  $\Lambda_\pi$  can be accommodated if additional vertex effects, such as correlated  $\pi\rho$  exchange, are incorporated<sup>59)</sup>). The large cut-off value results in a strong pion self-energy in nuclear matter which, in turn, needs to be tamed by short-range  $NN$  correlations which we implement via Migdal parameters ( $g'_{ij}$ ). To avoid premature pion condensation (i.e. at densities close to saturation), the  $g'$  parameters have to be rather large ( $\sim 0.8$ ) and, consequently, the pion self-energy is quite sensitive to their precise values. On the other hand, in the  $\rho$ -meson self-energy, the pion self-energy figures into the two-pion cloud of the  $\rho$ . As mentioned above, this part of the in-medium  $\rho$  self-energy has

<sup>\*)</sup> At finite temperature, direct interactions of the  $\rho$  with thermal pions can give rise to mesonic resonance excitations as in Fig. 3 (c), but they do not appear at zero temperature.



been constrained independently by relating its imaginary part in the low-density limit to: (i)  $\pi N \rightarrow \rho N$  production cross sections (which at high energy are dominated by pion exchange); (ii) the non-resonant continuum in nuclear photo-absorption (corresponding to processes of type  $\gamma N \rightarrow \pi N, \pi\Delta$ ). The first constraint puts a rather stringent limit on  $\Lambda_\pi$  of order 0.3 GeV, not to overshoot the experimental cross section (note that in these reactions one pion is on-shell). This situation is reminiscent to the elastic  $P$ -wave  $\pi N$  scattering phase shifts, where a  $\Delta$ -pole ansatz also requires a soft form-factor cut-off,  $\Lambda_{\pi N\Delta} \sim 0.3$  GeV (c.f., e.g., Refs. 60,61)). It turns out that, with this soft form-factor, the non-resonant background in nucleon photo-absorption [constraint (ii)] is predicted at  $\sim 80 \mu\text{b}$ , which is consistent with experiment (c.f., e.g., the discussion in Section 4.1.2 of Ref. 56)). The ‘unnatural’ softness of the  $\pi NN(\Delta)$  form-factor could be related to missing cancellations with higher resonances, or loop corrections to the vertex in a more elaborate treatment of the effective hadronic theory. Since the soft form-factor suppresses the in-medium ( $P$ -wave) pion self-energy appreciably, small Migdal parameters ( $\sim 0.2$  or even 0) are preferred in the application to photo-absorption on nuclei. Recently, this model for the in-medium  $\rho$  has been checked against data from the CLAS collaboration for nuclear photo-production of  $\rho$  mesons and dileptons.<sup>62)</sup> The agreement with experiment is good which corroborates the reliability of the  $\rho$ - $\pi$  modeling in nuclear matter. In the present calculation of the in-medium  $a_1$  resonance, the pion in the  $\pi\rho$  cloud is probed in very similar kinematics as in the  $\pi\pi$  cloud of the  $\rho$ . We therefore think that model B is, in fact, a more realistic and consistent parameter choice, whereas parameter set A should be considered as an ‘upper limit’ on the medium effects of the pion.

Finally, medium effects on the baryonic degrees of freedom of the model have been accounted for in a schematic way. The  $\rho$  self-energy model discussed above includes such modifications in terms of parametric in-medium widths for the nucleon and baryon resonances.<sup>57)</sup> The fit of these parameters to the photo-absorption spectra results in a small increase of the  $\Delta$  decay width and larger modifications for higher excitations (e.g., the  $N^*(1520)$  width is fitted with an in-medium broadening of 250 MeV at nuclear saturation density). The data provide no compelling evidence for baryon-mass shifts in nuclei, and therefore no in-medium mass corrections have been introduced for the baryons (rather than introducing, e.g., compensating mass shifts for the nucleon and the  $\Delta$  in  $\Delta h$  excitations). Of course, a more complete calculation would compute the baryon self-energies microscopically, but this is beyond the scope of the present paper. For consistency we have also incorporated these minimal (but empirically motivated) modifications of the nucleon and  $\Delta$  degrees of freedom into the pion self-energy in Eqs. (3.1,3.3). The effect on the pion propagator turns out to be small and can be safely neglected from a practical point of view in the evaluation of the  $\rho\pi$  cloud self-energy of the  $a_1$  (note that it represents changes of at least second order in density).

The in-medium pion and  $\rho$ -meson self-energies are implemented into the  $G_{\rho\pi}$  loop function by replacing the  $\rho$  and  $\pi$  propagators in Eq. (2.6) by their in-medium versions. The analytic structure of  $G_{\rho\pi}$  simplifies considerably by using the Lehmann

representation for the meson propagators,

$$D_{\pi(\rho)}(q^0, \vec{q}; \varrho) = \int_{-\infty}^{\infty} d\omega \frac{S_{\pi(\rho)}(\omega, \vec{q}; \varrho)}{q^0 - \omega + i\varepsilon}, \quad (3.4)$$

where  $S_{\pi(\rho)}(\omega, \vec{q}; \varrho)$  is the pion ( $\rho$ -meson) spectral function,

$$S_{\pi(\rho)}(\omega, \vec{q}; \varrho) = -\frac{1}{\pi} \text{Im} D_{\pi(\rho)}(\omega, \vec{q}; \varrho), \quad (3.5)$$

and

$$D_{\pi(\rho)}(q^0, \vec{q}; \varrho) = \frac{1}{(q^0)^2 - \vec{q}^2 - m_{\pi(\rho)}^2 - \Pi_{\pi(\rho)}(q^0, \vec{q}; \varrho)}. \quad (3.6)$$

After some manipulations, the  $\rho\pi$  loop function in nuclear matter takes the form

$$G_{\rho\pi}(P^0, \vec{P} = \vec{0}; \varrho) = \int_0^\infty \frac{dW}{2\pi} \left[ \frac{1}{P^0 - W + i\varepsilon} - \frac{1}{P^0 + W - i\varepsilon} \right] F(W) \quad (3.7)$$

with

$$F(W) = \int^{q_{\max}} \frac{d^3q}{(2\pi)^3} \int_{-W}^W du \pi S_{\pi}(E_+, \vec{q}; \varrho) S_{\rho}(E_-, \vec{q}; \varrho), \quad (3.8)$$

where  $E_{\pm} = (W \pm u)/2$ . Note that  $\text{Im} G_{\rho\pi}(P^0) = -F(P^0)/2$  and thus  $F$  plays the role of a generalized in-medium two-particle phase space. The cut-off regularization is applied in the three-momentum integral, Eq. (3.8), and thus  $F(W)$  depends explicitly on the cut-off parameter.

Eqs. (3.7) and (3.8) reduce to the vacuum expressions obtained in Ref. 22) for vanishing nuclear density,  $\varrho = 0$ . One just replaces the in-medium pion spectral function by  $S_{\pi}(\omega, \vec{q}; \varrho = 0) = \delta[\omega^2 - E_{\pi}(\vec{q})^2]$  and the  $\rho$ -meson propagator by  $D_{\rho}(\omega, \vec{q}; \varrho = 0) = [\omega^2 - E_{\rho}(\vec{q})^2 + iM_{\rho}\Gamma_{\pi\pi}]^{-1}$ , which accounts for its  $P$ -wave  $\pi\pi$  decay width,  $\Gamma_{\pi\pi} \simeq 150$  MeV in the center-of-mass system (CMS). The latter expression for the  $\rho$  propagator in vacuum neglects the real part of the  $\rho$  self-energy, which is reabsorbed in the physical  $\rho$  mass. In this work, however, consistent with the  $\rho$  self-energy model from Refs. 51), 57), we use the full  $\rho$  spectral function, which also accounts for the energy-dependence of the real part of the  $\rho$  self-energy both in vacuum and in the medium. For completeness, we quote the case of two stable particles in vacuum:  $F(P^0 = \sqrt{s}) = (4\pi)^{-1} q(s)/\sqrt{s} \theta(s - (M + m)^2)$ , with  $q(s)$  the on-shell momentum of each particle in the CMS.

It is instructive to compare our approach with earlier calculations of the in-medium  $a_1(1260)$  spectral function within many-body approaches. In Ref. 15) the role of the excitation of “meson”-sobars by the  $\rho$  and  $a_1$  mesons was studied. It was found that these mechanisms contribute to the mixing of the vector and axialvector correlators by inducing extra strength in the low-energy part of the  $a_1$  spectral function (see also Ref. 16)). In the present calculation, we do not account for “ $a_1$ -sobars” excitations ( $N^*h$  excitations with the quantum numbers of the  $a_1$ ). Nevertheless, as

will be seen in the next section, the  $a_1$  spectral function acquires low-energy strength from the coupling to in-medium  $\rho$  and  $\pi$  mesons. This coupling also lowers the inelastic threshold in the  $\rho\pi$  channel all the way to  $s = 0$ , in analogy to the in-medium  $\pi$  and  $\rho$ -meson spectral functions. The excitation of these low-energy modes induces a mixing of vector and axial correlators also in the absence of resonance-hole modes for the  $a_1$ .<sup>63),64)</sup> In particular, the modifications of the meson cloud can lead to a rather pronounced non-linear density dependence of their in-medium decay widths, especially if the vacuum threshold of the decay products is close to the parent's meson mass, e.g., for the  $\phi$  and  $\omega$ .<sup>65),66)</sup> Such effects have recently received considerable attention in experiment and theory.<sup>67)–70)</sup>

#### §4. $\pi\rho$ Correlations in Nuclear Matter

##### 4.1. Scattering Amplitudes

Let us start by exhibiting the previously calculated spectral functions for  $\pi$ - and  $\rho$ -mesons in cold nuclear matter which serve as an input for our further calculations. Figs. 5(a-f) summarize these quantities for the pion as a function of its energy for various 3-momenta and nuclear densities (in units of saturation density,  $\rho_0 = 0.16 \text{ fm}^{-3}$ ). As a reference, the arrows in the upper and middle panels represent the pole position ( $\delta$ -function like spectral functions) of the pion propagator in vacuum.

The pion spectral function clearly exhibits the different modes excited in the nuclear medium. At low momentum, the pion quasi-particle peak carries most of the strength together with a moderate contribution of the  $Nh$  excitations at lower energies. The  $\Delta h$  mode induce a sizable attraction on the pion mode relative to free space. In model A, at momenta of several hundred MeV/ $c$ , the excitation of the  $\Delta h$  becomes prominent and significantly broadens to the pion quasi-particle peak. The two models for the pion self-energy exhibit noticeable differences, mostly due to the different values for the form-factor cut-off parameter,  $\Lambda_\pi$ , see Eq. (3.2). For  $\Lambda_\pi = 1 \text{ GeV}$  (model A), sizable strength appears at low energies (in fact, in the space-like region,  $q_0 < q$ ) up to high momenta, arising from both the  $Nh$  mode and the quasi-pion mode. As density is increased (for a fixed momentum), the pion mode progressively approaches the  $\Delta h$  energy threshold and thus exhibits a narrower quasi-particle structure. Using a softer form-factor,  $\Lambda_\pi = 0.3 \text{ GeV}$  (model B), cuts down the pion self-energy already for a few hundred MeV of momentum. At  $q = 300 \text{ MeV}$ , the three-level structure of the self-energy is less visible, and the pion is characterized by a moderately broadened quasiparticle with considerable attraction, whereas little low-energy strength is induced by  $Nh$  excitations. At  $q = 500 \text{ MeV}$  the pion becomes a relatively narrow quasiparticle with strength concentrated around the free energy and a width increasing with density.

In the lower panels of Fig. 5 we show the  $\rho$ -meson spectral function<sup>14)</sup> as a function of  $M_I \equiv \sqrt{q^{02} - q^2}$ . The spectral function exhibits a strong broadening as density increases (with a slight upward mass shift for small 3-momentum). The shoulder structure at energies of around  $q_0 \simeq 600 \text{ MeV}$  is mostly due to the  $N^*(1520)h$

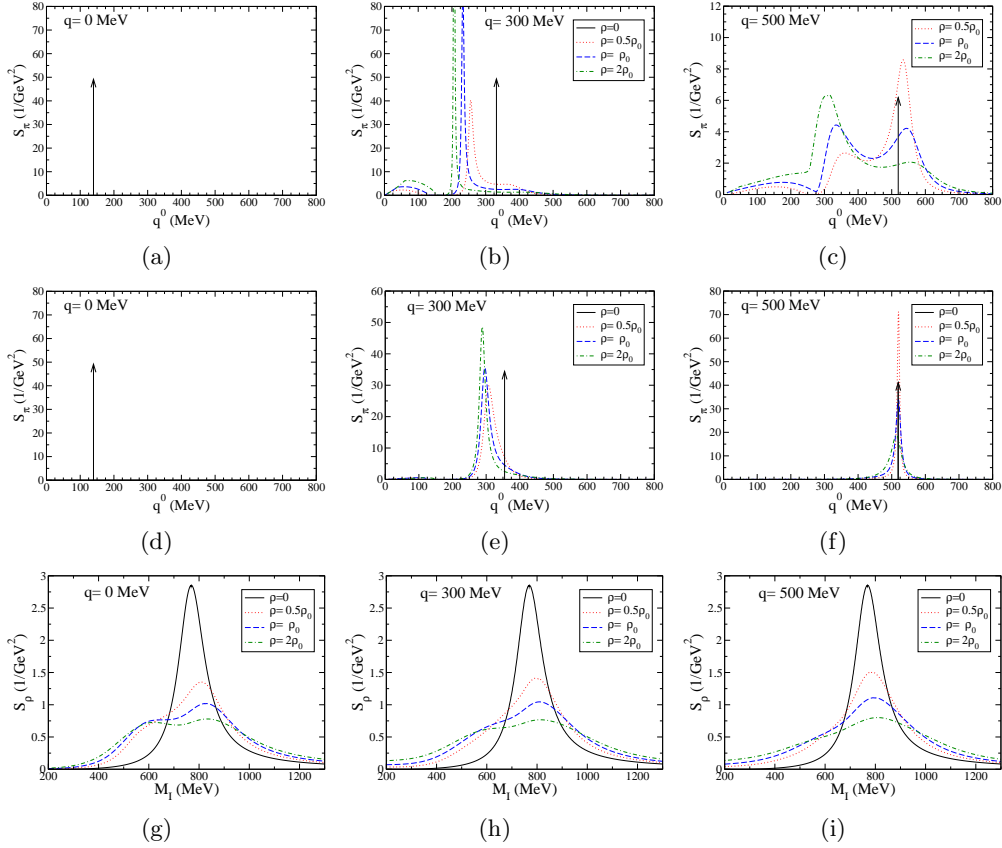


Fig. 5. Spectral functions for the  $\pi$  and  $\rho^{14)}$  for different nuclear densities and 3-momenta as indicated in the legends. The first (second) row corresponds to model A (B) for the  $\pi$ -self-energy. The  $\rho$  spectral function (third row) is plotted as a function of  $M_I \equiv \sqrt{q^{02} - q^2}$ .

excitations and collective  $\Delta h$  states in the pion cloud. This structure progressively fades away at higher momenta, whereas the broadening from in-medium pion-related channels persists at moderate momenta (it also reduces at momenta  $q \geq 1$  GeV, see, e.g., Ref. 62)).

We are now in position to inspect the consequences for the  $\rho\pi$  correlations, starting with the intermediate 2-particle propagator,  $G_{\rho\pi}(E)$ , shown in Fig. 6 for different nuclear densities and vanishing total 3-momentum. The upper (lower) panels have been obtained within model A (B) of the pion self-energy. The imaginary part,  $\text{Im} G_{\rho\pi}(E)$  (which we recall can be interpreted as a generalized  $\rho\pi$  phase space at finite density), exhibits a gradual movement of strength to lower energies with increasing density, cf. Fig. 6(a); this strength, in particular, extends to below  $E = 3m_\pi$ , which is the (absolute) vacuum threshold in this channel upon accounting for the  $\rho$  decay width into two pions. In Fig. 6(a) a large increase in phase space is visible, even at the vacuum “pole” mass of the  $a_1$  at  $E \simeq 1.1$  GeV, which is a direct consequence of the excitation of low energy modes by both the  $\rho$  and  $\pi$  mesons in the medium, corresponding, e.g., to  $a_1 N \rightarrow [\rho N] \rightarrow \pi\pi N$ ,  $a_1 N \rightarrow \pi N^*(1520)$ , etc. The

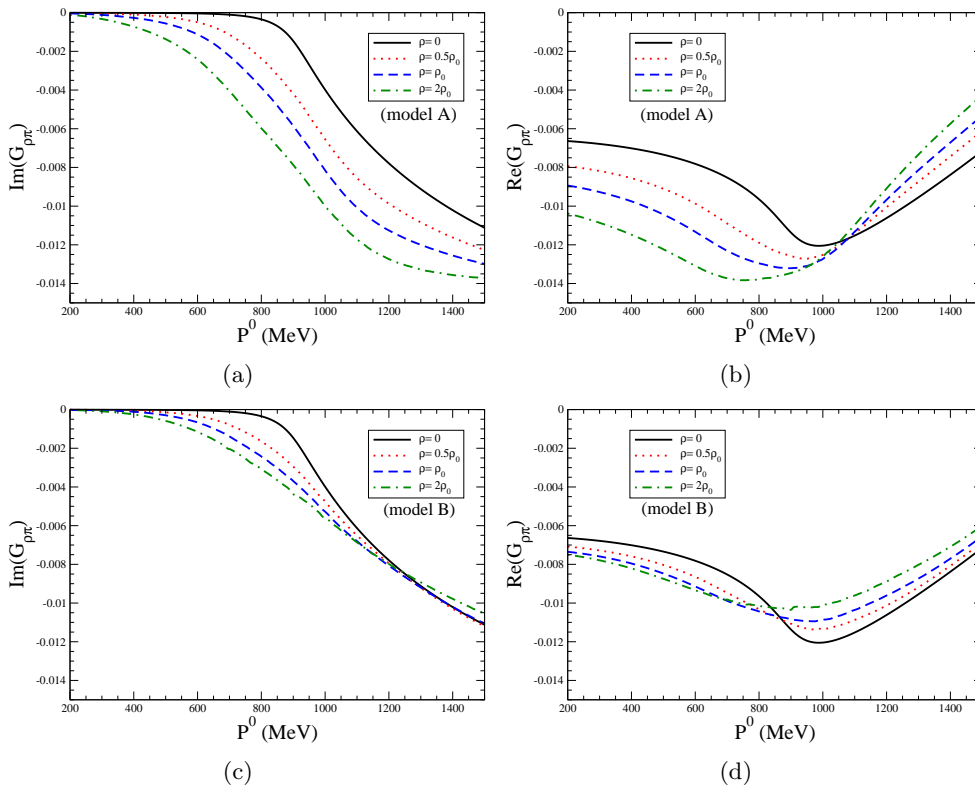


Fig. 6. Imaginary (left) and real (right) parts of the  $\pi\rho$  loop function, as a function of total energy at zero 3-momentum for different nuclear densities. The upper (lower) panels correspond to using model A (B) for the pion self-energy.

additional open channels increase the  $a_1(1260)$  decay probability in the medium as compared to the vacuum. Using  $\pi$  self-energy B, Fig. 6(c), the qualitative behavior of  $G_{\rho\pi}(E)$  is similar, however the changes with density are less pronounced, particularly around 1.2 GeV. The reason is the use of a softer pion form-factor, which reduces the effective phase space by cutting down the contribution from pion-related in-medium channels at high momenta, which are relevant at such large (total) energy. The results for  $\text{Im} G_{\rho\pi} = -F(E)/2$  can now be conveniently applied to compute the real part of  $G_{\rho\pi}$  via the principle value integral in Eq. (3.7). The results are depicted in the right panels of Fig. 6. One notices an increase in attraction at energies below 800 MeV with increasing the density, with an accompanying increase in repulsion above  $E \simeq 1$  GeV. We can expect that the latter will lead to a slight increase of the “nominal”  $a_1$  mass (or the peak of its spectral function) on the real energy-axis.

Before discussing modifications of the  $\pi\rho$  scattering amplitude in the medium, let us first briefly comment on the result in vacuum, cf. Fig. 7(a). In this case the “projection” of the  $a_1(1260)$  pole onto the real axis clearly manifests itself as a prominent resonance structure (also note the effect of the  $K\bar{K}^*$  threshold at around  $E = 1400$  MeV). One of the main reasons that renders the shape of the  $a_1(1260)$  resonance rather different from a Breit-Wigner function can be understood by com-

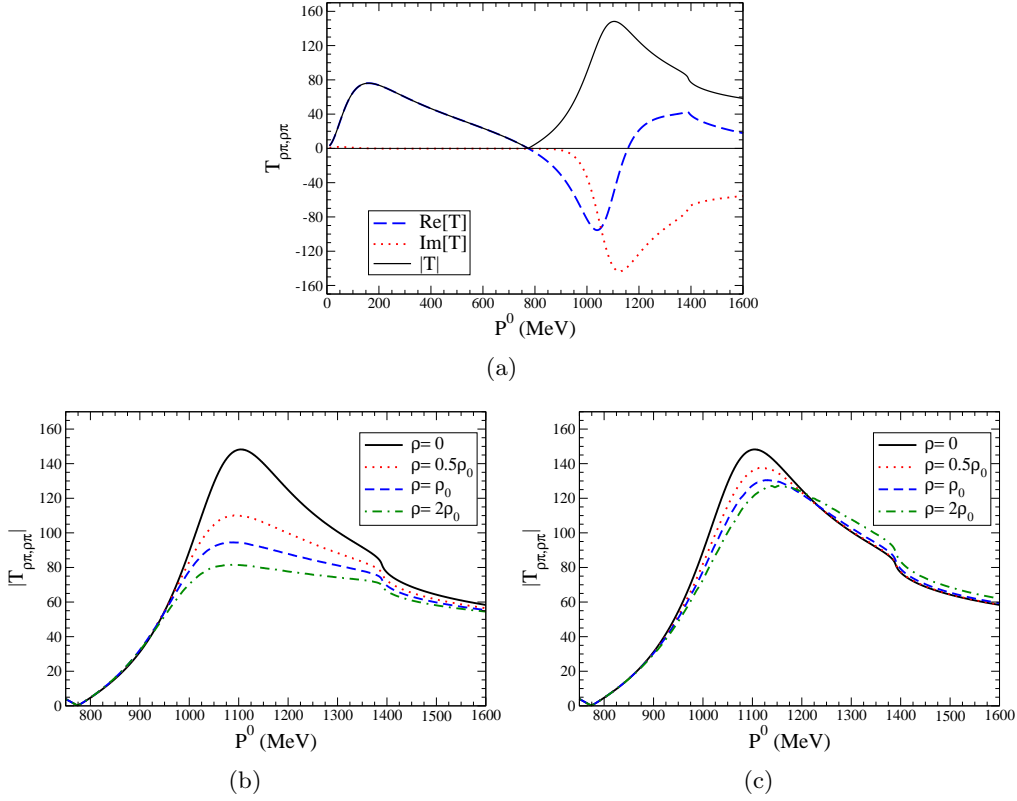


Fig. 7. Isospin  $I = 1$   $\rho\pi \rightarrow \rho\pi$  scattering amplitude. Upper panel: real part, imaginary part and modulus at zero density. Lower panels: modulus for different nuclear densities:  $\pi$ -self-energy A, panel (b);  $\pi$ -self-energy B, panel (c).

paring, in Fig. 7(a), the modulus (solid line), real (dashed line) and imaginary (dotted line) part of the  $\rho\pi \rightarrow \rho\pi$  scattering amplitude. The amplitude has a zero at 775 MeV induced by a zero in the  $\rho\pi$  tree level potential  $V$ , Eq. (2.4), around this energy, since the full amplitude is essentially (up to the  $K^*K$  channel) proportional to  $V$ , recall Eq. (2.5). However the pole contribution itself has a large strength at this energy. This means that the non-resonant contribution (background) is as large as the pole contribution but of opposite sign, actually canceling each other. As a consequence of the background, the final shape of the amplitude is distorted as compared to a pure pole contribution. All these effects are automatically generated within our non-perturbative unitary amplitudes. This is reminiscent to the case of the scalar-isoscalar  $\sigma(500)$  meson, where the presence of a subthreshold Adler zero (dictated by chiral symmetry) renders its shape rather different from a Breit-Wigner.<sup>71), 72)</sup> Thus, the large distance of the pole from the real axis and the presence of a zero at around 775 MeV are the main reasons for deviations from a conventional Breit-Wigner shape in Fig. 7. For further illustration we additionally display in Fig. 8 the modulus of the vacuum  $\pi\rho \rightarrow \pi\rho$  amplitude in the second Riemann sheet as a function of  $\text{Re}(P^0)$  and  $\text{Im}(P^0)$ , which exhibits the evolution of the shape of  $|T_{\rho\pi}|$

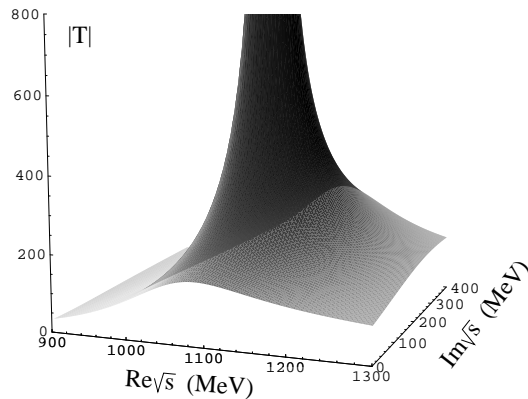


Fig. 8. Modulus of the  $\rho\pi \rightarrow \rho\pi$  scattering amplitude in isospin  $I = 1$  in the second Riemann sheet, showing the  $a_1(1260)$  pole and its projection onto the the real energy axis.

$\varrho/\varrho_0$	$\sqrt{s_0}$ (A)	$\sqrt{s_0}$ (B)
0	$1133 - 207i$	$1133 - 207i$
1/2	$1080 - 231i$	$1133 - 220i$
1	$1049 - 232i$	$1130 - 235i$
2	$1019 - 232i$	$1135 - 254i$

Table I. Density dependence of the  $a_1$ -pole position,  $\sqrt{s_0}$  (units are MeV). A and B stand for the  $\pi$ -self-energy model used in the calculation.

from the pole position to its (distorted) “projection” onto the real energy axis.

Let us now return to the nuclear medium effects of the  $\rho\pi \rightarrow \rho\pi$  scattering amplitude, the modulus of which is displayed for different densities in the lower panels of Fig. 7. Fig. 7(b) is evaluated with  $\pi$ -self-energy A and Fig. 7(c) with  $\pi$ -self-energy B. As density increases, the shape of the distribution around the  $a_1(1260)$  peak widens, especially in Fig. 7(b), following the phase-space argument given above. The position of the peak barely changes, again following the variations in the real part of  $G_{\rho\pi}$ , which has a moderate energy dependence around the “nominal” pole mass. Overall, the resonant structure present in free space tends to dissolve in the nuclear medium, which is in the spirit of the “melting resonance” scenario of chiral symmetry restoration, reminiscent to hadronic many-body calculations of the  $\rho$  meson.<sup>5),14)</sup> We shall elaborate further on this assertion in the next section by studying the first Weinberg sum rule (WSR) at finite nuclear density.

We can also evaluate the dependence of the  $a_1$  pole position with the nuclear density. The results are shown in Table I for the two different pion-self-energy parameterizations, A and B. The broadening with density visible in Fig. 7(b) for the scattering amplitude is reflected in the imaginary part of the pole position only up to about a density of  $\varrho \simeq 0.5\varrho_0$ ; at higher densities, the suppression of  $|T_{\rho\pi}|$  seems to play an important role. Using the  $\pi$ -self-energy B, the broadening with density is more manifest while the real part remains essentially constant. However, once again, one should be aware that the  $a_1$  pole lies far from the real axis, and therefore the correspondence between the imaginary part of the pole position and

the width of the associated distribution (spectral function) of the resonance on the real energy axis is not direct. Interestingly, the density evolution of the real part of the  $a_1$  pole indicates a slight shift to lower energies, whereas the  $\rho$ -meson spectral distribution is actually pushed to slightly higher energies (mostly as a consequence of two-level repulsion with resonance-hole modes and a collective  $\Delta h$  mode in the pion cloud), cf. Fig 5. It is tempting to speculate that the mutual approach of the two poles (vector and axialvector) is related to a precursor of chiral restoration, i.e., in addition to a “melting” of the vector and axialvector spectral functions, our results may suggest an additional trend toward “mass degeneracy”. Its effect, however, is largely superseded by the large widths,  $\Gamma_{\rho, a_1}^{\text{med}} \gg |E_{\rho}^{\text{pole}} - E_{a_1}^{\text{pole}}|$ .

#### 4.2. Evaluation of in-Medium Weinberg Sum Rules

An expected precursor phenomenon of chiral symmetry restoration is a reduction of the pion decay constant,  $f$  (an order parameter of chiral symmetry breaking), as nuclear density increases. Since  $f$  can be interpreted as the pion-pole strength figuring into the (longitudinal) axialvector current, its vanishing can be realized via a degeneracy of the vector and axialvector current-current correlation functions if chiral symmetry is restored in the medium. The Weinberg sum rules (WSRs) relate the pion decay constant to energy weighted moments of the difference between vector and axialvector spectral functions. In particular, in vacuum, the first WSR reads<sup>73)</sup>

$$\int \frac{ds}{s} (\hat{S}_V - \hat{S}_A) = f^2. \quad (4.1)$$

In our normalization,  $\hat{S}_V$  in Eq. (4.1) is related to the vector spectral function,  $S_V$ , by  $\hat{S}_V = (sF_V/M_V)^2 S_V$ .

The generalization of the first WSR in the medium is given in Ref.,<sup>74)</sup>

$$\int_0^\infty \frac{\omega d\omega}{\omega^2 - \vec{p}^2} (\hat{S}_V^L(\omega, \vec{p}) - \hat{S}_A^L(\omega, \vec{p})) = 0. \quad (4.2)$$

Here, only the longitudinal components contribute to the sum rule, and we work in the rest frame of the nuclear medium. Separating out the pionic contributions from the axialvector correlator, we consider first the vector and axialvector meson contributions with  $\vec{p} = 0$ . For the zero momentum limit, the longitudinal components become degenerate with the transverse ones, which we have calculated in the previous sections. The low-energy vector correlator is dominated by the contribution of the  $\rho$  meson,  $S_V \simeq S_\rho$ . Similarly, the axialvector correlator is usually considered to be largely saturated by the axialvector meson,<sup>75)</sup> as depicted diagrammatically in Fig. 9(a). A proper evaluation of the axialvector spectral function at all energies requires a lengthy calculation as well as a correct matching to the perturbative QCD continuum. In Ref. 46) the low-energy part of the spectrum has been worked out for the vacuum case, in a model calculation with dynamically generated axialvector mesons similar to the one presented here. Implementing the full calculation of the axialvector spectral function and extending it to account for nuclear medium effects is out of the scope of the present work. However, we can make a simple estimation of the WSR by using the one-pole approximation of the vector and axialvector spectral



functions. For the pionic contributions, we work in the chiral limit ( $m_\pi=0$  also in the medium). One has to keep in mind, however, that the pion is not the only zero mode in the nuclear medium, but the particle-hole excitations with zero energy can contribute to the axialvector correlator.<sup>76)</sup> Thus, in general, the right-hand-side of the WSR in the nuclear medium is given by the summation of all zero-mode contributions (pion and particle-hole excitations). It has been shown, however, that in the linear density approximation, only the pion branch contributes to the axialvector correlator.<sup>76)</sup> The longitudinal component of the axialvector correlator with  $\vec{p} = 0$  has only the  $\mu\nu=00$  component, which involves the time component of the pion decay constant,  $f_t$ .

An approximate expression for the WSR at zero three-momentum can be obtained from Eq. (4.2) by considering saturation of the correlators by narrow  $\rho$  and  $a_1$  resonances, as

$$F_V^2 - F_A^2 \simeq f_t^2, \quad (4.3)$$

where  $F_V$  is the coupling of the vector-meson resonance to the vector current and  $F_A$  is the coupling of the axialvector resonance to the axial current. One has to be aware that these assumptions are only fulfilled approximately since the  $a_1$  is quite broad and the axial correlator may be influenced by non-resonant contributions. Indeed, in Ref. 46), in a study of  $\tau$  decays into three pions, it was shown that there is a strong interference of the  $a_1$  resonance contribution with other non-resonant terms in the evaluation of the vacuum axialvector spectral function.

Next we define within our approach an effective axial coupling constant,  $F_A$ , estimate its density dependence and thus the density dependence of  $f_t$ . A similar idea was used in Ref. 31) in a study of the  $N_c$ -dependence of dynamically generated axialvector resonances within the constraints of WSR's.

The definition and normalization of the  $F_A$  and  $F_V$  couplings in our formalism are similar to the standard case when explicit axialvector fields,  $A_\mu$ , are considered in the theory:

$$\mathcal{L}_{V\phi} = -\frac{F_V}{\sqrt{2}M_V} \langle \partial_\mu V_\nu f_+^{\mu\nu} \rangle, \quad (4.4)$$

$$\mathcal{L}_{A\phi} = -\frac{F_A}{\sqrt{2}M_A} \langle \partial_\mu A_\nu f_-^{\mu\nu} \rangle \quad (4.5)$$

(given in an equivalent form in Ref. 77) with antisymmetric tensors for the vector meson fields) with

$$\begin{aligned} f_\pm^{\mu\nu} &= u F_L^{\mu\nu} u^\dagger \pm u^\dagger F_R^{\mu\nu} u, \\ F_L^{\mu\nu} &= \partial^\mu l^\nu - \partial^\nu l^\mu - i[l^\mu, l^\nu], \\ F_R^{\mu\nu} &= \partial^\mu r^\nu - \partial^\nu r^\mu - i[r^\mu, r^\nu], \\ r^\mu &= v^\mu + a^\mu, \quad l^\mu = v^\mu - a^\mu. \end{aligned} \quad (4.6)$$

We refer to Ref. 77) for an explicit definition and normalization of the different terms in Eq. (4.6). Expanding  $f_\pm^{\mu\nu}$  up to one pseudoscalar meson field, the former

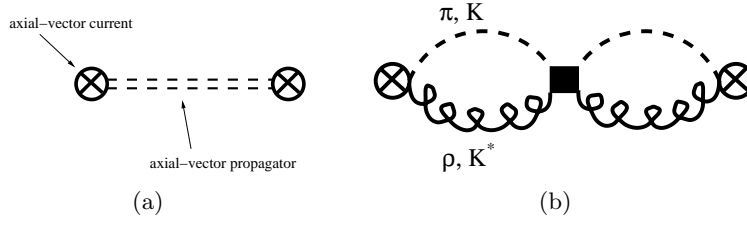


Fig. 9. Axialvector two point correlation function. (a): for an explicit  $a_1(1260)$  field. (b): for a dynamically generated  $a_1(1260)$  resonance. The square represents the  $VP \rightarrow VP$  unitarized interaction.

Lagrangians provide the coupling of the explicit axialvector resonance field,  $A_\mu$ , to an axialvector current,  $a_\mu$ , through  $F_A$  and the coupling of a  $VP$  pair to the same current via  $F_V$ . Note that the coupling of an axialvector current to a  $VP$  pair also receives a contribution from the Lagrangian<sup>77)</sup>

$$\mathcal{L} = -i \frac{\sqrt{2}G_V}{M_V} \langle \partial_\mu V_\nu u^\mu u^\nu \rangle \quad (4.7)$$

with

$$u^\mu = iu^\dagger D_\mu U u^\dagger, \quad (4.8)$$

$$D_\mu = \partial_\mu U - i(v_\mu + a_\mu)U + iU(v_\mu - a_\mu) \quad (4.9)$$

and  $U = u^2$ .

If we had an explicit axialvector field, one could evaluate the two-point axialvector correlation function from the diagram in Fig. 9(a), using the  $F_A$  coupling in Eq. (4.5). Since in our scheme the axialvector resonances are dynamically generated they do not appear as explicit fields in the Lagrangian. Still, the axial resonance is linked to the axialvector current-current correlator via a  $VP$  loop, as depicted in Fig. 9(b). We note that the evaluation of the full axialvector spectral function includes other non-resonant contributions (like, for instance, the uncorrelated  $3\pi$  and  $\rho\pi$  continuum). However, for the WSR in the one-pole approximation, Eq. (4.3), the diagram in Fig. 9(b) is the dominant contribution around the  $a_1(1260)$  pole.

Matching the contributions to the axialvector correlator from the diagrams in Figs. 9(a) and 9(b) evaluated at the  $a_1$  pole, we obtain

$$F_A = \frac{\sqrt{2}M_A}{f} \frac{1}{s} \left[ \frac{1}{M_\rho} \left( \left( \frac{F_V}{2} - G_V \right) (s + m_\rho^2 - m_\pi^2) + 2G_V m_\rho^2 \right) G_{\rho\pi}(s) g_{\rho\pi} \right. \\ \left. - \frac{1}{\sqrt{2}m_{K^*}^*} \left( \left( \frac{F_V}{2} - G_V \right) (s + m_{K^*}^2 - m_K^2) + 2G_V M_{K^*}^2 \right) G_{K^*K}(s) g_{K^*K} \right] \quad (4.10)$$

where  $G_{\rho\pi}(s)$  and  $G_{K^*K}(s)$  arise from the  $VP$  loops [see Eq. (2.6)] in Fig. 9(b),  $g_{\rho\pi}$  is the effective coupling constant of the dynamically generated  $a_1(1260)$  to  $\rho\pi$  for isospin  $I = 1$ , and  $g_{K^*K}$  the one to the  $1/\sqrt{2}(|\bar{K}^*K\rangle - |K^*\bar{K}\rangle)$  negative  $G$ -parity state. These couplings, including their relative phase, are a natural output of the chiral unitary approach and are obtained from the residues of the  $\rho\pi \rightarrow \rho\pi$

and  $\rho\pi \rightarrow K^*K$  amplitudes at the resonance pole.<sup>22)</sup> For the numerical evaluation of Eq. (4.10), we take  $M_A = \text{Re}(\sqrt{s_{pole}})$ . Eq. (4.10) provides, in general, complex values for  $F_A$  since both  $G_l$  and the effective couplings are generally complex. In order to compare with the coupling,  $F_A$ , defined in Eq. (4.5) (which may have a different phase), we take in the following for  $F_A$  in Eq. (4.10) its absolute value.

For the results presented in the former section we have used a cut-off parameter of  $q_{\max} \sim 1$  GeV; similar results are obtained by varying  $q_{\max}$  around 1 GeV within reasonable values. However, to reproduce the empirical value of  $f$ , a quantitative numerical matching between  $F_V$  and  $F_A$  is required (the difference of  $F_V^2$  and  $F_A^2$  appears in Eq. (4.3)). We do this by exploiting the latitude in  $q_{\max}$  (our only free parameter) and fix it at  $q_{\max} \sim 0.835$  GeV to obtain  $f = 93$  MeV at zero density. This simple one-pole estimate shows that it is possible to accommodate the Weinberg sum rule in vacuum within our approach.

The couplings  $F_V$  and  $G_V$  will in general also pick up a nuclear-density dependence. The estimate of this dependence in our framework has large uncertainties, mostly due to the pole approximation that we are considering. We have checked that estimating of  $F_V$  from the residue of the  $\rho$  meson pole results in a slight increase of  $F_V$  with density. However, this estimate is blurred due to the presence of the resonance-hole structure close to the  $\rho$  mass. Another possibility is to recast the  $\rho$  spectral function in a two-level model, similar to what was done in Ref 15), and then apply the narrow-resonance limit. Again this produces a small variation in  $F_V$ . All these pole-dominance estimations suffer from the fact that they ignore the non-trivial structure of the meson spectral function on the real axis. With these uncertainties in mind, we have adopted a (conservative) estimation of the density dependence of  $F_V$  of the form  $F_V = F_V^{(0)}(1 \pm 0.2\rho/\rho_0)$ , where  $F_V^{(0)}$  is the vacuum value of the coupling constant; that is, we allow for variations up to 20% at normal nuclear matter densities. Furthermore we have assumed the same amount of uncertainty in the value of  $G_V$  to allow for possible medium modifications encoded in this coupling. For the numerical calculation we have used  $F_V = 156$  MeV and  $G_V = 69$  MeV at zero density.

Before discussing the numerical results, an explanation of the role played by chiral symmetry in the  $\pi$  self-energy model entering both the  $\rho$  and  $a_1$  meson clouds is in order. Our pion self-energy is solely due to  $P$ -wave  $\pi N$  interactions, operating in both isospin  $\frac{1}{2}$  ( $\pi N \rightarrow N$ ) and  $\frac{3}{2}$  ( $\pi N \rightarrow \Delta$ ) channels. The isospin-averaged  $S$ -wave  $\pi N$  scattering length is very small (a consequence of chiral symmetry). Therefore,  $S$ -wave pion self-energy contributions are small in symmetric nuclear matter and have been neglected in our work. At the minimal level, the vanishing of the  $\pi N$  interaction in the soft pion limit ( $q \rightarrow 0$ ) is compatible with basic chiral requirements, while the  $\Delta$ -nucleon-hole model is well established phenomenologically (we note that the chiral structure of baryon resonances is still an open problem<sup>78)–81)</sup>). Regarding short-range correlations in the pion self-energy, chiral counting in the  $NN$  interaction is more involved (especially with one-pion exchange). In this work, when using parameter set A, we rely on the simplest possible 4-point interaction to remedy premature pion condensation. In our preferred set B, there is almost no sensitivity to the short-range

$\varrho/\varrho_0$	present work ( $\pi$ -self-energy A)	present work ( $\pi$ -self-energy B)	ref. <sup>15)</sup>	ref. <sup>82)</sup>	ref. <sup>83)</sup>
0	93	93	93	93	93
1/2	100-108	91-101	65-78	87	81
1	65-86	66-93	52-67	79	69

Table II. Density dependence of the pion decay constant  $f$ , quoted in units of MeV. The ranges in the columns designated “present work” represent the variation due to possible density dependences of  $F_V$  and  $G_V$ .

$NN$  correlations, which evades the problem of chiral constraints in the  $NN$  sector. We emphasize that the main goal of the Weinberg sum-rule analysis in this section is to provide a consistent interpretation of our hadronic, many-body description of the  $a_1$  interactions with the nuclear medium in terms of chiral symmetry restoration. A similar line of thought has been followed in Ref. 76), where an in-medium sum rule for the quark condensate has been derived in terms of the hadronic matrix elements of all the zero modes present in nuclear matter (such as in-medium quasi-pions and  $Nh$  excitations). This implies that not only the pion modes but also the nuclear many-body modes contribute to the modification of the quark condensate in the nuclear medium.

In Table II we summarize results of  $f$  as a function of density for the two- $\pi$  self-energy models considered in the present work. The intervals shown in the “present work” columns represent uncertainties from the density dependence of  $F_V$  and  $G_V$  as delineated above. For comparison we show in the last three columns results from Refs. 15), 82), 83). Our result for  $f$  at  $\varrho = \varrho_0$  is compatible with the general trend from previous calculations, namely, a decrease with density, in agreement with the expectation from a partial restoration of chiral symmetry in the nuclear medium. This seems not to be the case at  $\varrho = \varrho_0/2$ . This may be due to our schematic form of the axialvector correlator and that the WSR is estimated at the  $a_1$  pole and hence it does not account for the full structure of the meson spectral function. We recall that a significant background (which our model provides but which is not relevant at the pole position) is present, which, e.g., produces a zero at about 800 MeV in the scattering amplitude. Its interference with other non-resonant contributions<sup>46)</sup> notably affects the shape of the axialvector spectral function. Furthermore, since  $f$  is obtained from a subtle subtraction between  $F_V^2$  and  $F_A^2$  in Eq. (4.3), small variations in the estimation of  $F_A$  can produce appreciable differences in  $f$ . Therefore, in order to draw more reliable conclusions on the restoration of the chiral symmetry using the Weinberg sum rule, a more detailed analysis beyond the one pole approximation used here is called for, utilizing the full vector and axialvector spectral functions on the real axis (including non-resonant contributions). Further work in this direction, as well as an extension of the present calculation to finite temperatures (as relevant in the phenomenology of heavy-ion collisions), is in progress.

## §5. Conclusions

We have performed a theoretical estimation of the properties of the  $a_1(1260)$  axialvector resonance in cold nuclear matter. The starting point was a chiral unitary approach in which the vacuum  $a_1(1260)$  is generated dynamically via resumming four-point interactions of a vector and a pseudoscalar meson in a coupled channel framework. In this way, the  $a_1(1260)$ , along with most of the low-lying axialvector resonances, appears as a pole of the scattering amplitude in the complex energy plane, which is reflected by a resonant structure on the real (physical) energy axis. The model does not include the axialvector meson as an explicit field. The underlying four-point interaction vertices are given by the lowest order chiral Lagrangian, with one free parameter required as a regularization scale for the one-loop two-particle propagator.

Medium effects on the  $\rho\pi$  amplitude have been investigated by implementing  $\rho$  and  $\pi$  self-energies in cold nuclear matter, as obtained from well established hadronic many-body calculations. The meson self-energies figure into the scattering amplitude through the  $VP$  loop function, thereby modifying the available phase space for the  $a_1$  resonance decay due to opening of additional channels in the nuclear medium, e.g.,  $a_1N \rightarrow [\rho N] \rightarrow \pi\pi N$  or  $a_1N \rightarrow \pi N^*(1520)$ .

In the  $a_1(1260)$  resonance region the  $VP$  amplitude exhibits a broadening with increasing density, which could be indicative for a “resonance melting” scenario. Even though less pronounced, we also found indications for an increase (decrease) of the  $\rho$  ( $a_1$ ) meson quasiparticle mass with density, which could suggest a tendency toward “mass degeneracy”. The relations of both mechanisms to chiral symmetry restoration in the vector / axialvector system at finite density remain to be understood.

We have furthermore given a prescription to study the density dependence of the pion decay constant utilizing the first Weinberg sum rule in a one-pole approximation. The main observations from this study are: (i) In the vacuum, within a chiral unitary model, the dynamically generated  $a_1$  resonance enables to reproduce the Weinberg sum rule by adjusting the regularization parameter of the  $VP$  loop integral at “natural” magnitude; and, (ii) With increasing nuclear density, the pion decay constant tends to decrease, as a consequence of the “admixture” of in-medium vector and pseudoscalar modes. Our analysis of the WSR is not very conclusive at present due to the approximations involved in our calculation. However, it provides a starting point for more elaborate evaluations using the full meson spectral functions on the real energy axis. In addition, the implementation of a chiral scheme for baryon resonance excitations, as well as a self-consistent treatment of vector-axialvector mixing, is required for more definite conclusions. These challenges will be addressed in future work.

## Acknowledgments

This work is partly supported by DGICYT contracts FIS2006-03438, FPA2007-62777 and FPA2008-00592, the Fundación Séneca contract 02975/PI/05, the EU

Integrated Infrastructure Initiative Hadron Physics Project under Grant Agreement n.227431, the UCM-BSCH contract GR58/08 910309 and the Grant-in-Aid for the Global COE Program “The Next Generation of Physics, Spun from Universality and Emergence” from MEXT of Japan. D.J. acknowledges support from the Grant-in-Aid for Scientific Research by Monbu-Kagaku-Sho of Japan (Nos. 20028004 and 20540273). This work was partially done under the Yukawa International Program for Quark-Hadron Physics. D.C. wishes to acknowledge financial support from the “Juan de la Cierva” Programme (Ministerio de Ciencia e Innovación, Spain). R.R. was supported by a U.S. National Science Foundation CAREER award under grant PHY-0449489.

### References

- 1) R. Rapp, R. Machleidt, J. W. Durso and G. E. Brown, *Phys. Rev. Lett.* **82** (1999) 1827.
- 2) F. Weber, R. Negreiros and P. Rosenfield, arXiv:0705.2708 [astro-ph].
- 3) B. A. Li, L. W. Chen and C. M. Ko, *Phys. Rept.* **464** (2008) 113
- 4) R. S. Hayano and T. Hatsuda, arXiv:0812.1702 [nucl-ex].
- 5) R. Rapp, J. Wambach, and H. van Hees, *Landolt Börnstein, New Series I/23-A* (2010), in press; and arXiv:0901.3289 [hep-ph].
- 6) V. Metag, *Prog. Theor. Phys. Suppl.* **168** (2007) 503.
- 7) C. Djalali, R. Nasseripour, D. Weygand and M. Wood [CLAS Collaboration], *Prog. Theor. Phys. Suppl.* **168** (2007) 511.
- 8) A. Starostin et al. (Crystal Ball Collaboration), *Phys. Rev. Lett.* **85**, (2000) 5539.
- 9) N. Grión et al. (CHAOS Collaboration), *Nucl. Phys. A* **763** (2005) 80.
- 10) D. Adamova *et al.* (CERES/NA45 Collaboration), *Phys. Lett. B* **666** (2008) 425.
- 11) Y. C. Pachmayer *et al.* [HADES Collaboration], *J. Phys. G* **35** (2008) 104159.
- 12) R. Arnaldi *et al.* [NA60 Collaboration], *Eur. Phys. J. C* **61** (2009) 711.
- 13) M. Harada and K. Yamawaki, *Phys. Rept.* **381** (2003) 1.
- 14) R. Rapp and J. Wambach, *Eur. Phys. J. A* **6** (1999) 415.
- 15) Y. Kim, R. Rapp, G.E. Brown and M. Rho, *Phys. Rev. C* **62** (2000) 015202.
- 16) R. Rapp, *Eur. Phys. J. A* **18** (2003) 459.
- 17) M. Urban, M. Buballa and J. Wambach, *Nucl. Phys. A* **697** (2002) 338.
- 18) M. Harada, C. Sasaki and W. Weise, *Phys. Rev. D* **78** (2008) 114003.
- 19) S. Strüber and D. H. Rischke, *Phys. Rev. D* **77** (2008) 085004.
- 20) R.D. Pisarski, *Phys. Rev. D* **52** (1995) 3773.
- 21) M.F.M. Lutz and E.E. Kolomeitsev, *Nucl. Phys. A* **730** (2004) 392.
- 22) L. Roca, E. Oset and J. Singh, *Phys. Rev. D* **72** (2005) 014002.
- 23) L.S. Geng, E. Oset, L. Roca and J. A. Oller, *Phys. Rev. D* **75** (2007) 014017.
- 24) A. Dobado and J.R. Pelaez, *Phys. Rev. D* **56** (1997) 3057.
- 25) J.A. Oller and E. Oset, *Nucl. Phys. A* **620** (1997) 438 [Erratum-*ibid.* A **652** (1999) 407].
- 26) J.A. Oller, E. Oset and J.R. Pelaez, *Phys. Rev. D* **59** (1999) 074001 [Erratum-*ibid.* D **60** (1999) 099906].
- 27) J.A. Oller and E. Oset, *Phys. Rev. D* **60** (1999) 074023.
- 28) N. Kaiser, P.B. Siegel and W. Weise, *Nucl. Phys. A* **594** (1995) 325.
- 29) J.A. Oller and U.G. Meissner, *Phys. Lett. B* **500** (2001) 263.
- 30) M.F.M. Lutz and E.E. Kolomeitsev, *Nucl. Phys. A* **700** (2002) 193.
- 31) L.S. Geng, E. Oset, J.R. Pelaez and L. Roca, *Eur. Phys. J. A* **39** (2009) 81.
- 32) N. Kaiser, *Eur. Phys. J. A* **3** (1998) 307.
- 33) J. Nieves and E. Ruiz Arriola, *Nucl. Phys. A* **679** (2000) 57.
- 34) D. Gamermann, E. Oset, D. Strottman and M.J. Vicente Vacas, *Phys. Rev. D* **76** (2007) 074016.
- 35) E. Oset and A. Ramos, *Nucl. Phys. A* **635** (1998) 99.
- 36) C. Garcia-Recio, M.F.M. Lutz and J. Nieves, *Phys. Lett. B* **582** (2004) 49.
- 37) T. Hyodo, S.I. Nam, D. Jido and A. Hosaka, *Phys. Rev. C* **68** (2003) 018201; T. Hyodo, S.I. Nam, D. Jido and A. Hosaka, *Prog. Theor. Phys.* **112** (2004) 73.
- 38) D. Jido, J.A. Oller, E. Oset, A. Ramos and U.G. Meissner, *Nucl. Phys. A* **725** (2003) 181.

- 39) J.A. Oller, Eur. Phys. J. A **28** (2006) 63.
- 40) S. Sarkar, E. Oset and M.J. Vicente Vacas, Nucl. Phys. A **750** (2005) 294 [Erratum-ibid. A **780** (2006) 78].
- 41) T. Hyodo, D. Jido and L. Roca, Phys. Rev. D **77** (2008) 056010; L. Roca, T. Hyodo and D. Jido, Nucl. Phys. A **809** (2008) 65.
- 42) T. Hyodo, D. Jido and A. Hosaka, Phys. Rev. C **78** (2008) 025203.
- 43) S. Weinberg, Phys. Rev. **166** (1968) 1568; S. Coleman, J. Wess and B. Zumino, Phys. Rev. **177** (1969) 2239; C.G. Callan, S. Coleman, J. Wess and B. Zumino, ibid. 2247.
- 44) M.C. Birse, Z. Phys. A **355** (1996) 231.
- 45) M. Wagner and S. Leupold, Phys. Lett. B **670** (2008) 22.
- 46) M. Wagner and S. Leupold, Phys. Rev. D **78** (2008) 053001.
- 47) S. Schael *et al.* [ALEPH Collaboration], Phys. Rept. **421** (2005) 191.
- 48) D.M. Asner *et al.* [CLEO Collaboration], Phys. Rev. D **61** (2000) 012002.
- 49) G. Chanfray and P. Schuck, Nucl. Phys. A **555** (1993) 329.
- 50) M. Herrmann, B.L. Friman and W. Nörenberg, Nucl. Phys. A **560** (1993) 411.
- 51) M. Urban, M. Buballa, R. Rapp and J. Wambach, Nucl. Phys. A **641** (1998) 433.
- 52) H.C. Chiang, E. Oset and M. J. Vicente-Vacas, Nucl. Phys. A **644** (1998) 77.
- 53) E. Oset, H. Toki and W. Weise, Phys. Rept. **83** (1982) 281.
- 54) A.B. Migdal, E.E. Saperstein, M.A. Troitsky and D.N. Voskresensky, Phys. Rept. **192** (1990) 179.
- 55) E. Oset, P. Fernandez de Cordoba, L. L. Salcedo and R. Brockmann, Phys. Rept. **188** (1990) 79.
- 56) R. Rapp and J. Wambach, Adv. Nucl. Phys. **25** (2000) 1.
- 57) R. Rapp, M. Urban, M. Buballa and J. Wambach, Phys. Lett. B **417** (1998) 1.
- 58) M. Urban, M. Buballa, R. Rapp and J. Wambach, Nucl. Phys. A **673** (2000) 357.
- 59) G. Janssen, J.W. Durso, K. Holinde, B.C. Pearce and J. Speth, Phys. Rev. Lett. **71** (1993) 1978.
- 60) E.J. Moniz, Nucl. Phys. A **354** (1981) 535C.
- 61) H. van Hees and R. Rapp, Phys. Lett. B **606** (2005) 59.
- 62) F. Riek, R. Rapp, T. S. Lee and Y. Oh, Phys. Lett. B **677** (2009) 116.
- 63) B. Krippa, Phys. Lett. B **427** (1998) 13.
- 64) G. Chanfray, J. Delorme, M. Ericson, and M. Rosa-Clot, Phys. Lett. B **455** (1999) 39.
- 65) D. Cabrera and M. J. Vicente Vacas, Phys. Rev. C **67** (2003) 045203.
- 66) D. Cabrera and R. Rapp, *in preparation*.
- 67) D. Cabrera, L. Roca, E. Oset, H. Toki and M.J. Vicente Vacas, Nucl. Phys. A **733** (2004) 130.
- 68) T. Ishikawa *et al.*, Phys. Lett. B **608** (2005) 215.
- 69) M. Kaskulov, E. Hernandez and E. Oset, Eur. Phys. J. A **31** (2007) 245.
- 70) M. Kotulla *et al.* [CBELSA/TAPS Collaboration], Phys. Rev. Lett. **100** (2008) 192302.
- 71) J. A. Oller, Phys. Rev. D **71** (2005) 054030.
- 72) L. Roca, J.E. Palomar, E. Oset and H.C. Chiang, Nucl. Phys. A **744** (2004) 127.
- 73) S. Weinberg, Phys. Rev. Lett. **18** (1967) 507.
- 74) J. I. Kapusta and E. V. Shuryak, Phys. Rev. D **49** (1994) 4694.
- 75) J. F. Donoghue and E. Golowich, Phys. Rev. D **49** (1994) 1513.
- 76) D. Jido, T. Hatsuda and T. Kunihiro, Phys. Lett. B **670** (2008) 109.
- 77) G. Ecker, J. Gasser, A. Pich and E. de Rafael, Nucl. Phys. B **321** (1989) 311.
- 78) C.E. Detar and T. Kunihiro, Phys. Rev. D **39** (1989) 2805.
- 79) D. Jido, Y. Nemoto, M. Oka and A. Hosaka, Nucl. Phys. A **671** (2000) 471.
- 80) D. Jido, T. Hatsuda and T. Kunihiro, Phys. Rev. Lett. **84** (2000) 3252.
- 81) D. Jido, M. Oka and A. Hosaka, Prog. Theor. Phys. **106** (2001) 873.
- 82) D. Davesne, Y.J. Zhang, G. Chanfray and J. Wambach, arXiv:nucl-th/0002032.
- 83) V. Thorsson and A. Wirzba, Nucl. Phys. A **589** (1995) 633; U.G. Meissner, J.A. Oller and A. Wirzba, Annals Phys. **297** (2002) 27.